Highlights

Design of an UWA-OTFS Communication Receiver Based on Single-Element Two-Dimensional Virtual Passive Reversal

Yang Yang, Lu Ma, Boon-Chong Seet, Songzuo Liu, Siang Ma

- Proposed a novel receiver architecture for UWA-OTFS communication using 2D-VPR technology in the delay-Doppler domain to enhance reliability.

- Developed a BOMP-DPW channel estimator to facilitate 2D-VPR equalization, thereby enhancing main lobe energy concentration and achieving a reduction in raw BER by an order of magnitude.

- Reliable communication was achieved in sea trials with a data rate of 1.8 kbps, a towing distance of $0 - 5$ km, and a relative speed of 2 m/s.

Design of an UWA-OTFS Communication Receiver Based on Single-Element Two-Dimensional Virtual Passive Reversal

Yang Yang[a,b,c], Lu Ma[a,b,c,d,*], Boon-Chong Seet[e], Songzuo Liu[a,b,c,d], Siang Ma[a,b,c]

[a]National Key Laboratory of Underwater Acoustic Technology, Harbin Engineering University, Harbin, 150001, China
[b]Key Laboratory of Marine Information Acquisition and Security (Harbin Engineering University), Ministry of Industry and Information Technology, Harbin, 150001, China
[c]College of Underwater Acoustic Engineering, Harbin Engineering University, Harbin, 150001, China
[d]Sanya Nanhai Innovation and Development Base of Harbin Engineering University, Sanya, 572024, China
[e]Department of Electrical and Electronic Engineering, Auckland University of Technology, Auckland, 1010, New Zealand

Abstract

Orthogonal Time Frequency Space (OTFS) modulation offers a novel solution to enhance the reliability of mobile underwater acoustic (UWA) communication systems. In this study, a receiver architecture tailored for UWA-OTFS communication is presented, leveraging single-element two-dimensional virtual passive reversal (2D-VPR) technology in the delay-Doppler (DD) domain. To enhance the concentration of main lobe energy in the equivalent channel after 2D-VPR equalization, a block orthogonal matching pursuit with dynamic power weighting (BOMP-DPW) channel estimator is proposed, resulting in an order-of-magnitude reduction in the communication system's raw bit error rate (BER). Furthermore, considering the impact of signal distortion and noise, the 2D-VPR processor driven by the BOMP-DPW estimator is coupled with a minimum mean square error (MMSE) equalizer to further suppress sidelobe interference and noise. The proposed scheme was tested in the South China Sea, where data processing results confirmed that the receiver achieved reliable communication within a frequency band of $2-4$ kHz, a data rate of 1.8 kbps, a maximum towing distance of 5 km, and a relative speed of 2 m/s between the transmitter and receiver.

Keywords: Underwater acoustic communication, OTFS, Virtual passive time reversal, Two dimensional, BOMP

1. Introduction

The orthogonal time-frequency space (OTFS) modulation technique maps signals in the delay-Doppler (DD) domain [1], effectively utilizing the sparse characteristics of the channel, exhibiting excellent resistance to multipath and Doppler effects [2], and providing a new solution for the stability of mobile underwater acoustic (UWA) communication [3, 4]. However, real UWA channels exhibit severe multipath effects, frequency-selective fading, Doppler spreading, and limited channel bandwidth [5–7]. Such features lead to significant spreading of UWA channels in the DD domain, making it a key challenge to harness the benefits of OTFS modulation and develop efficient and robust receiver designs [8].

Currently, the design of UWA-OTFS communication receivers in most literature is limited to simulation validation [9–13], while experimental validation remains relatively rare [4, 14]. The proposed equalization methods include nonlinear techniques such as Turbo iterative equalization [4, 15], message passing (MP) receivers [16, 17], and deep learning-based approaches [18, 19], as well as enhanced linear-complexity minimum mean square error (MMSE) equalization methods [11]. It is worth mentioning that UWA array signal processing can improve reception gain [20], while time-reversal mirror array processing enables effective space-time-frequency focusing [21]. A two-dimensional passive time-reversal decision feedback equalizer receiver operating in the DD domain has been proposed in the literature [3]. However, as it relies on array processing, it is overly burdensome and difficult to apply in practical UWA communication systems that prioritize simple nodes and low power consumption [22].

In comparison to array-based processing, a single-element time reversal mirror significantly reduces device complexity, thereby enhancing the feasibility of time reversal mirror technology for UWA communication [23, 24]. However, this simplification also imposes higher demands on channel estimation accuracy [3]. In response to the block sparsity characteristics of UWA channels in the DD domain, the block orthogonal matching pursuit (BOMP) channel estimator can estimate path blocks and obtain sparse path block estimation results [25]. On the other hand, the single-element time-reversal mirror can only utilize multipath signals between two nodes and cannot achieve spatial focusing gain, which increases sidelobe energy after reversal [21]. Thus, in UWA-OTFS communication, key challenges for single-element two-dimensional virtual passive reversal (2D-VPR) technology in the DD domain include improving channel estimation accuracy, enhancing the concentration of main lobe energy, and suppressing sidelobe energy leakage.

This paper proposes a single-input single-output (SISO)

*Corresponding author
Email address: malu@hrbeu.edu.cn (Lu Ma)

UWA-OTFS communication system, which effectively enhances the main lobe energy concentration after the 2D-VPR equalizer in the delay-Doppler (DD) domain. The main contributions of this work are as follows:

- A novel UWA-OTFS receiver design is presented, utilizing single-element two-dimensional time-reversal technology. This design focuses the main path in the two-dimensional delay and Doppler domains, effectively mitigating inter-Doppler interference (IDI) caused by the spreading of UWA wideband signals in the DD domain.
- A block orthogonal matching pursuit with a dynamic power weighting (BOMP-DPW) channel estimator is developed for precise channel estimation, effectively suppressing sidelobe energy on both sides of the main peak. Meanwhile, the single-element design simplifies the complexity of time-reversal mirror array processing equipment.
- Sea towing experiments at different transmission depths fully verified the reliability of the underwater OTFS communication system receiver design proposed in this paper. The 2D-VPR processor driven by the BOMP-DPW estimator is coupled with a MMSE equalizer, enabling all transmitted data to be successfully decoded through the LDPC decoder.

The remainder of this paper is organized as follows: Section 2 describes the UWA-OTFS system model, Section 3 details the receiver design based on 2D-VPR, and Section 4 and Section 5 present the simulation results and sea trial experiments, respectively. Finally, conclusions are drawn in Section 6.

2. UWA-OTFS System model

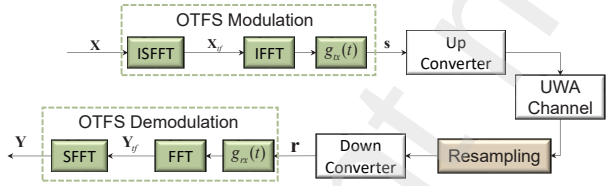

Fig. 1. System model for OTFS.

At the transmitter, NM information symbols are selected from the modulation alphabet $\mathrm{A} = \{a_1, ..., a_Q\}$. They are arranged in the DD domain matrix $\mathbf{X} \in \mathbb{C}^{M\times N}$. Subsequently, the time-frequency domain sample matrix is obtained via the inverse symplectic finite Fourier transform (ISFFT). It can be expressed as

$$\mathbf{X}_{tf} = \mathbf{F}_M \cdot \mathbf{X} \cdot \mathbf{F}_N^{\dagger} \tag{1}$$

where $\mathbf{F}_M, \mathbf{F}_N^{\dagger}$ represent the M-point fast Fourier transform (FFT) and N-point inverse fast Fourier transform (IFFT) matrix, respectively.

The matrix $\mathbf{X}_{tf} \in \mathbb{C}^{M\times N}$ in the time-frequency domain is transformed into the delay-time domain sample matrix $\tilde{\mathbf{X}} \in \mathbb{C}^{M\times N}$ via an M-point IFFT,

$$\tilde{\mathbf{X}} = \mathbf{F}_M^{\dagger} \cdot \mathbf{X}_{tf} \tag{2}$$

After applying transmit pulse shaping to the delay-time domain sample matrix $\tilde{\mathbf{X}}$, it is vectorized to obtain a time-domain sample vector of length MN,

$$\mathbf{s} = vec(\mathbf{G}_{tx} \cdot \tilde{\mathbf{X}}) \in \mathbb{C}^{MN\times 1} \tag{3}$$

For a rectangular window, the pulse shaping function is defined as $\mathbf{G}_{tx} = \mathbf{I}_M$. The time-domain sample vector is converted from digital to analog, resulting in $s(t)$, which is then upconverted to a passband time-domain signal and transmitted through the UWA channel.

At the receiver, the passband sampled signal is obtained, and the Doppler factor is estimated using the synchronization header, followed by preliminary Doppler compensation via resampling. Subsequently, the signal is downconverted to yield the NM-point baseband received signal $\mathbf{r} \in \mathbb{C}^{MN\times 1}$, which is converted into the delay-time matrix $\tilde{\mathbf{Y}} \in \mathbb{C}^{M\times N}$.

$$\tilde{\mathbf{Y}} = \mathbf{G}_{rx} \cdot (vec_{M,N}^{-1}(\mathbf{r})) \tag{4}$$

The operation $vec_{M,N}^{-1}(\mathbf{r})$ transforms $\mathbf{r}$ into an $M\times N$ matrix, with the receive pulse shaping matrix defined as $\mathbf{G}_{rx} = \mathbf{I}_M$.

Then, the time-frequency domain received sampling matrix $\mathbf{Y}_{tf} \in \mathbb{C}^{M\times N}$ is obtained through an M-point FFT operation

$$\mathbf{Y}_{tf} = \mathbf{F}_M \cdot \tilde{\mathbf{Y}} \tag{5}$$

A symplectic finite Fourier transform (SFFT) operation is executed to derive the DD domain symbol $\mathbf{Y}$, represented as

$$\mathbf{Y} = \mathbf{F}_M^{\dagger} \cdot \mathbf{Y}_{tf} \cdot \mathbf{F}_N \tag{6}$$

The l-th row, n-th column element of the DD domain received matrix $\mathbf{Y} \in \mathbb{C}^{M\times N}$ is represented by $\mathbf{Y}_{l,k}$, where $l = 0, \ldots, M-1$ and $k = 0, \ldots, N-1$. $\mathbf{H}$ stands for the DD domain channel matrix, and the input and output relationship in the DD domain follow a two-dimensional circular convolution relationship, expressed as

$$\mathbf{Y}_{l,k} = \sum_{l'=0}^{M-1} \sum_{k'=0}^{N-1} \mathbf{H}_{[l-l']_M,[k-k']_N} \mathbf{X}_{l',k'}. \tag{7}$$

3. The proposed receiver

This section proposes a receiver design scheme for UWA-OTFS. The BOMP signal estimation method dynamically adjusts the weighting factors based on the estimated path block power to achieve main path focusing. Additionally, a cascaded MMSE equalizer is employed at the back end to mitigate IDI caused by sidelobes.

The processing flow at the receiver is illustrated in Fig. 2. First, the bandpass time-domain sampled signal is processed using linear frequency modulation (LFM) correlation to estimate

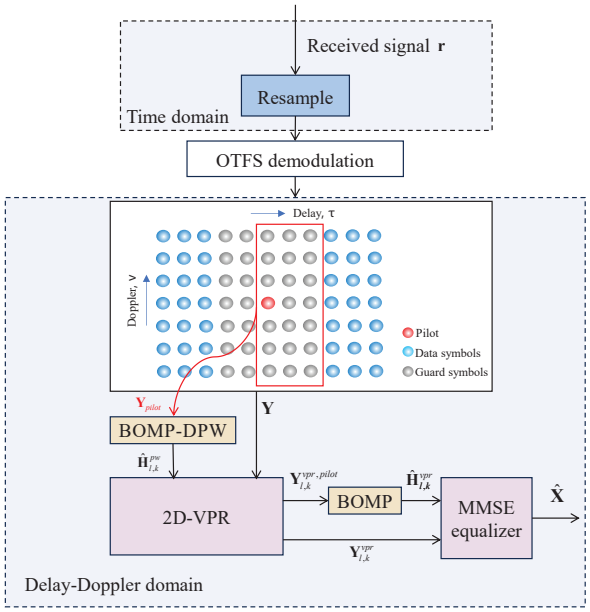

Fig. 2. Processing flow of the receiver in the DD domain.

Doppler factors, and Doppler pre-compensation is performed through resampling. Despite this, residual Doppler factors may remain [26], leading to IDI in the DD domain. The 2D-VPR operation can achieve symbol focusing in the DD domain, further mitigating the effect of residual Doppler factors. OTFS demodulation transforms the time-domain signal into the DD domain signal $\mathbf{Y}$. In the DD domain, the pilot symbols $\mathbf{Y}_{pilot}$ are first extracted to estimate channel state information (CSI). **Algorithm 1** outlines the BOMP-DWP channel estimation method, where the sensing matrix $\mathbf{\Phi}$ is derived by cyclically shifting the pilot symbols $\mathbf{Y}_{pilot}$, the observation vector $\mathbf{y}$ corresponds to the received signal, the signal sparsity is P, and the block approximation parameter w determines the size of the path block, which is determined by Doppler domain resolution, typically set to 3. These parameters are input to the channel estimator, with a detailed explanation of BOMP provided in reference [25]. Differently, to enable the recombined channel for driving the 2D-VPR, the power P_n of the current path weight $\hat{\mathrm{I}}_n(\xi_n)$ is estimated, and the channel matrix is reconstructed based on the power of various path blocks, aiming to enhance the main lobe and suppress sidelobes.

After the channel estimator BOMP-DPW outputs the estimated results $\hat{\mathbf{H}}_{l,k}^{pw}$, the estimated channel matrix $\hat{\mathbf{H}}_{l,k}^{pw}$ is first rotated by 180° as a whole, and the complex conjugate operation is applied, resulting in the two-dimensional time-reversal matrix $\hat{\mathbf{H}}_{l,k}^{pw,vpr}$

$$\hat{\mathbf{H}}_{l,k}^{pw,vpr} = conj\left(\hat{\mathbf{H}}_{M-l+1,N-k+1}^{pw}\right) \tag{8}$$

Substituting Eq. (7), Eq. (8) is rewritten as

$$\mathbf{Y}_{l,k}^{vpr} = \sum_{l'=0}^{L-1}\sum_{k'=0}^{N-1} \mathbf{X}_{l',k'} \mathrm{N}_{[l-l']_M,[k-k']_N} \tag{9}$$

Algorithm 1 BOMP-DPW channel estimation algorithm.

Input: $\mathbf{\Phi}$, $\mathbf{y}$, P, ω

Initialization: $\mathbf{r}_0 = \mathbf{y}$, $\Lambda_0 = \emptyset$, $n = 1$

While $n <= P$

do

1) Block Selection: $\lambda_n \leftarrow \arg\max_{j=1,\ldots,L} \left|\left\langle \mathbf{r}_{n-1}, \mathbf{x}_j \right\rangle\right|$

2) Block Support Extension:
$\xi_n = \{\lambda_n - \omega, \ldots, \lambda_n + \omega\}$, $\Lambda_n = \Lambda_{n-1} \cup \xi_n$

3) Channel Estimation:
$\hat{\mathrm{I}}_n(\xi_n) = \left(\mathbf{\Phi}(\xi_n)^T \mathbf{\Phi}(\xi_n)\right)^{-1} \mathbf{\Phi}(\xi_n)^T \mathbf{y}(\xi_n)$,
$\hat{\mathbf{h}}_n(\Lambda_n) = \left(\mathbf{\Phi}(\Lambda_n)^T \mathbf{\Phi}(\Lambda_n)\right)^{-1} \mathbf{\Phi}(\Lambda_n)^T \mathbf{y}(\Lambda_n)$

4) Power of path: $P_n = \int \left|\hat{\mathrm{I}}_n(\xi_n)\right|^2 d_{\xi_n}$,

5) Residual Update: $\mathbf{r}_n = \mathbf{y} - \mathbf{\Phi}\hat{\mathbf{h}}_n$

6) Convergence Check:
$\max \left\|\mathbf{\Phi}^H \mathbf{r}_{n-1}\right\| \geq 4 \times \arg\max \left\|\mathbf{\Phi}^H \mathbf{r}_{n-1}\right\|$

$n = n + 1$

end

7) Reorganization Channel:
$\hat{\mathbf{H}}_{l,k}^{pw} = \sum_n \left(P_n \times \hat{\mathrm{I}}_n(\xi_n) \middle/ \sum_n P_n\right)$

Output: $\hat{\mathbf{H}}_{l,k}^{pw}$

where

$$\mathrm{N}_{[l-l']_M,[k-k']_N} = \sum_{l=0}^{M-1}\sum_{k=0}^{N-1} \mathbf{H}_{[l-l']_M,[k-k']_N}^{pw} \mathbf{H}_{[l-l']_M,[k-k']_N}^{pw,vpr}. \tag{10}$$

In ideal conditions, all multipath components are focused on a single target point, forming a narrow main lobe. However, due to noise or interference, practical applications may lead to the emergence of sidelobes and the dispersion of the main lobe focus. To address this, the 2D-VPR equalized pilot position $\mathbf{Y}_{l,k}^{vpr,pilot}$ is extracted, the channel estimation $\hat{\mathbf{H}}_{l,k}^{vpr}$ is obtained through BOMP, and the MMSE equalizer is employed to further suppress the impact of sidelobes, producing the estimated symbols $\hat{\mathbf{X}}$.

4. Simulations

In this section, the UWA simulation channel is generated using the BELLHOP tool. The sound speed profile (SSP) of the UWA channel is derived from the South China Sea in October 2023. The transmitter depth is 15 m from the water surface, and the receiver depth is 40 m. The SSP and CSI are shown in Fig. 3. The relative velocity between the transmitter and receiver is denoted as v_0 m/s, while the velocity of the pth path is represented by v_p m/s. To model a time-varying channel, the velocity for each path is randomly selected from a uniform distribution spanning the range $[v_0 - \sqrt{3}\sigma_v, v_0 + \sqrt{3}\sigma_v]$ m/s, resulting in a standard deviation of σ_v m/s. Here, v_0 is set to 2 m/s, and σ_v varies between 0.1 and 0.3 m/s for channels incorporat-

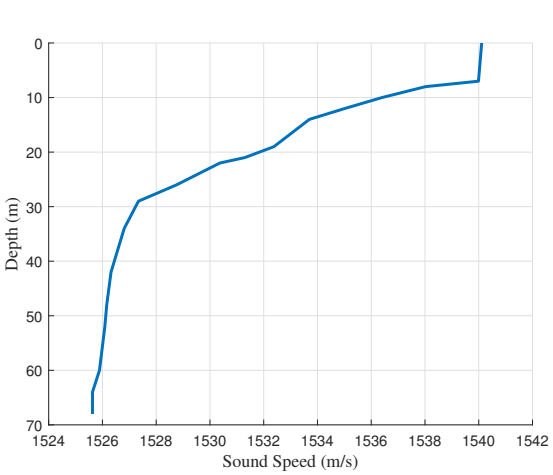

(a) SSP of South China Sea

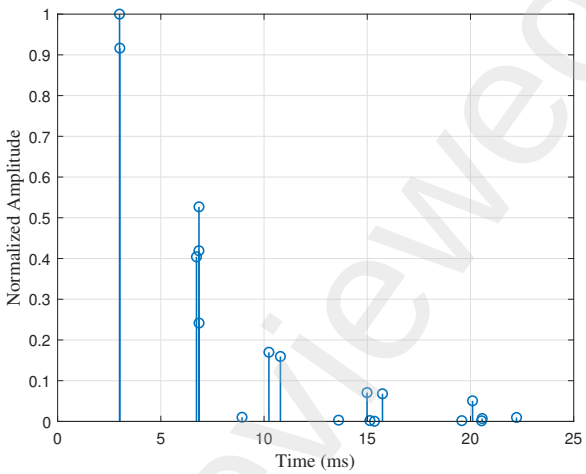

(b) CSI for simulation

Fig. 3. Conditions of the simulation channel.

ing path-specific Doppler scaling. The OTFS communication parameters are detailed in Table 1.

Table 1
Parameters of OTFS

Parameter	Value	Parameter	Value
Number of delay symbol	$M = 256$	Sample frequency	$f_s = 96kHz$
Number of Doppler symbol	$N = 24$	Cyclic prefix	$T_{cp} = 300ms$
Bandwith	$B = 2kHz$	Pilot utilization rate	$1/2$
Center frequency	$f_c = 3kHz$	Communication rate	$1.8kbps$

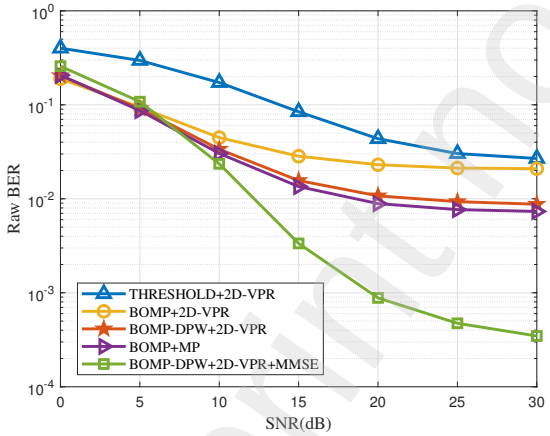

Fig. 4. Performance comparison of the raw BER for different receiver algorithms.

Fig. 4 illustrates a comparison of the raw BER performance under different receiver algorithms. Regarding channel estimation, the raw BER performance of threshold detection [27], BOMP, and BOMP-DPW estimators was evaluated when combined with 2D-VPR technology. The BOMP-DPW algorithm significantly reduces the raw BER from 10^{-1} to 10^{-2} by efficiently mitigating sidelobe interference. For channel equalization, the MP interference cancellation algorithm [2] was added, and the BER performance of the proposed BOMP-DPW+2D-VPR receiver is comparable to the BOMP+MP receiver. Additionally, the MMSE cascade following the 2D-VPR technique effectively suppresses sidelobe interference caused by channel estimation errors and noise.

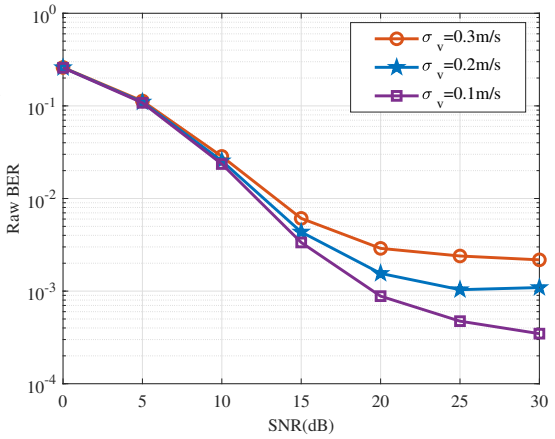

Fig. 5. The impact of Doppler spread on the raw BER performance of the proposed receiver.

Fig. 5 shows the comparison of the raw BER performance for UWA channels with Doppler factor variances $\sigma_v = 0.1, 0.2, 0.3$. The demodulation procedure is referenced in Fig. 2. The raw BER performance is significantly impacted by Doppler factor expansion, as the time-domain resampling operation only compensates for the average Doppler factor across all paths. As the variance of the Doppler factor increases, larger residual Doppler factors remain after resampling, leading to greater expansion in the Doppler domain grid and even in the delay domain grid, thereby limiting the focusing performance of 2D-VPR.

5. Sea field experiment results and analysis

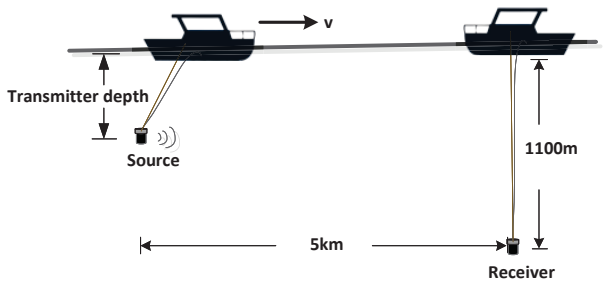

Fig. 6. Experimental scenario diagram.

An experiment was conducted in the South China Sea in 2024 to validate the effectiveness of the UWA-OTFS receiver. During the experiment, the hydrophones on the receiving side were placed near the sound channel axis to ensure high-quality signal reception, as illustrated in Fig. 6. The transmitter was towed back and forth at a speed of 2 m/s across a distance range of 0 to 5 km, starting at an initial distance of 5 km. Upon returning to the starting point, the transmitter's towing depth was adjusted to 350 m and 80 m, completing signal emission experiments under different depth conditions. Two back-and-forth towing experiments were conducted at these different transmission depths, resulting in two sets of experimental data, labeled as A and B.

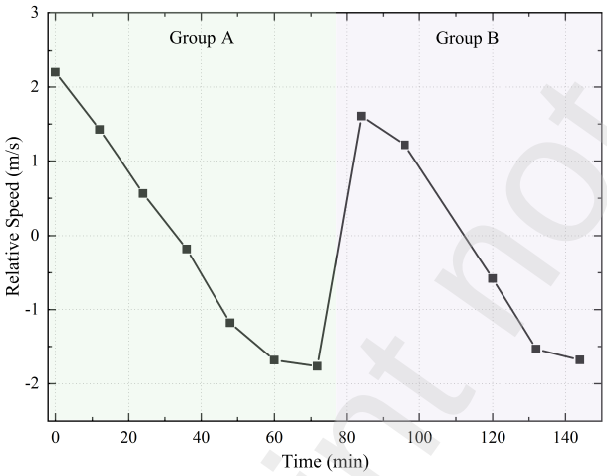

Fig. 7. Estimated relative speed of the two ships.

The transmitter continuously sent data packets, with the OTFS parameters for each packet configured as shown in Table 1. The maximum estimated channel delay range was 32 ms. Furthermore, LDPC decoding was performed on the MMSE output. The communication rate before decoding was 1.8 kbps, which was reduced to 0.9 kbps after 1/2 LDPC decoding. group A transmitted 28 data packets, and group B transmitted 20 data packets. In both test scenarios, the two vessels started 5 km apart, initially moving toward each other and later gradually separating. Relative velocities were recorded every 12 minutes using an LFM synchronization preamble, as shown in Fig.7.

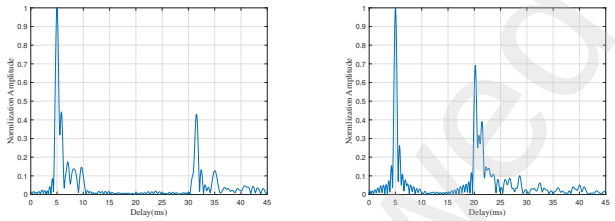

(a) CSI of group A (b) CSI of group B

Fig. 8. Estimated CSI of different group.

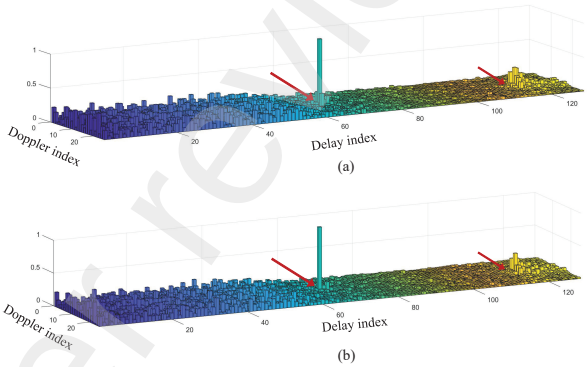

Fig. 9. Received Symbols in DD domain. (a) Before 2D-PTR Equalization (b) After 2D-PTR Equalization

Due to the differences in transmission depths, the UWA channel during the two groups also varied. The CSI estimated based on LFM correlation at different depths is shown in Fig. 8. In group A, the delay spread was 30 ms, while in group B, the delay spread was approximately 20 ms, consisting of two distinct path clusters. Fig. 9 shows a comparison of the DD domain received signal for one data packet before and after 2D-VPR equalization. The positions marked by the red arrows indicate the pilot symbols' shift and spread in the DD domain after passing through the channel, which contains real information about the UWA channel. In Fig. 9(b), the received signal after 2D-VPR equalization still shows the presence of sidelobes. Nevertheless, the main path with strong energy achieves excellent focusing in both the Doppler and delay domains. Although sidelobes persist, the application of power weighted operations reduces their amplitude, resulting in minor symbol interference. The subsequent cascaded MMSE equalizer effectively mitigates the interference caused by these sidelobes.

Fig. 10 shows the constellation diagrams before and after MMSE equalization. The sidelobes shown in Fig. 10 led to IDI, causing large deviations from the standard constellation values in Fig. 10 (a) before equalization. After applying the MMSE equalizer, IDI was effectively mitigated, resulting in more concentrated constellation points and reduced decision errors.

Fig. 11 shows the BER results for 48 transmitted data packets during the communication experiment. It compares the BER performance of three receiver algorithms: BOMP+2D-VPR+MMSE, BOMP-DPW+2D-VPR+MMSE, and BOMP-DPW+2D-VPR+MMSE+LDPC. The 2D-VPR equalization al-

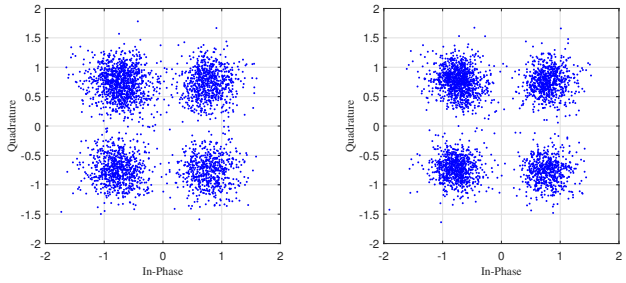

(a) Before equalization (b) After equalization

Fig. 10. Constellation diagrams before and after MMSE equalization.

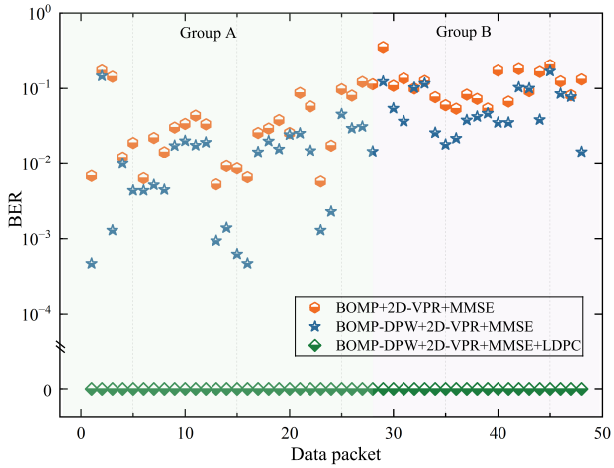

Fig. 11. BER analysis of 48 data packets.

gorithm, driven by BOMP-DPW, shows a significant improvement in BER performance. After LDPC decoding, the BER for all packets reaches 0.

Fig. 12 shows a comparison of the raw BER percentages for three receiver frameworks: I -the proposed BOMP-DPW+2D-VPR+MMSE receiver design, II - the BOMP+MP receiver design, and III - the OFDM communication system based on the time-reversal algorithm. Algorithm III refers to the current mature orthogonal frequency division multiplexing (OFDM) communication system. It performs time-reversal in the time domain, uses OMP for channel estimation, and applies cascaded frequency-domain equalization to achieve the original BER results. Residual Doppler factors in the received signal after time-domain resampling cause fractional Doppler effects in the DD domain, which limits the equalization performance of the MP algorithm. On the other hand, 2D-VPR equalization focuses the spread path energy onto the main path (as shown in Fig. 9), effectively mitigating the IDI caused by residual Doppler factors in the DD domain. It is worth noting that the overall decoding performance of group A is better than that of group B. This is due to differences in channel conditions caused by transmission depth. For the 2D-VPR algorithm, sparse and distinct multi-path components in the channel, where a few dominant paths account for most of the energy and the delay intervals between

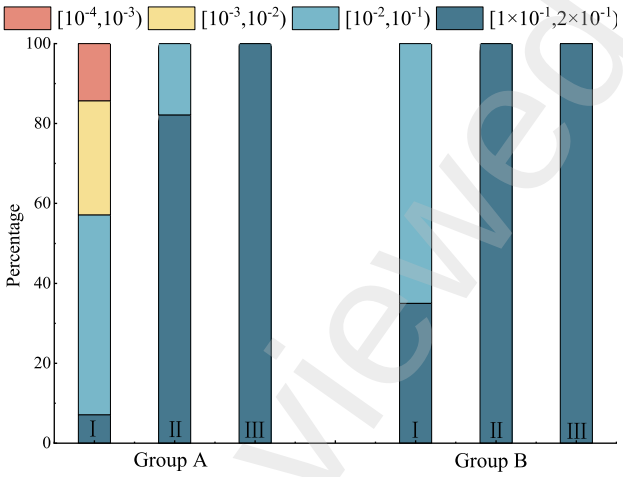

Fig. 12. BER percentages for different communication schemes and receivers.

paths are longer, are more favorable for the algorithm to accurately focus the energy of the main path. Furthermore, if the channel delay spread exceeds the maximum delay estimation range defined by the OTFS communication parameters, or if the receiver cannot synchronize with the first path of the UWA channel, the receiver's performance will be constrained.

6. Conclusion

In this study, we propose a comprehensive receiver architecture for UWA-OTFS communication systems. The channel estimates produced by the BOMP-DPW algorithm are applied to 2D reversal equalization, effectively focusing the equivalent channel's main path in both the delay and Doppler domains. The combination of the 2D-VPR and MMSE equalizers mitigates residual sidelobes, achieving a dual interference suppression mechanism. Sea trial experiments validated the applicability of the 2D-VPR technique for UWA-OTFS communication systems, demonstrating stable communication at a relative speed of 2 m/s, a data rate of 1.8 kbps, and a towing distance of 0 – 5 km.

Declaration of competing interest

The authors declare that they have no known competing financial interests or personal relationships that could have appeared to influence the work reported in this paper.

Data availability

Data will be made available on request.

Acknowledgments

This research was supported in part by the National Key Research and Development Program of China under Grant 2023YFC3010800, in part by the National Natural Science

Foundation of China under Grant 62271161, in part by the Key Research and Development Program of Shandong Province under Grant 2022CXGC020409, and in part by the National Key Laboratory of Underwater Acoustic Technology under Grant 2023-JCJQ-LB-072-08. The work of Yang Yang was supported by the Chinese Scholarship Council (CSC).

References

[1] R. Hadani, S. Rakib, M. Tsatsanis, A. Monk, A. J. Goldsmith, A. F. Molisch, R. Calderbank, Orthogonal Time Frequency Space Modulation, in: Proc. IEEE Wireless Commun. Netw. Conf. (WCNC), IEEE, 2017, pp. 1–6.

[2] P. Raviteja, K. T. Phan, Y. Hong, E. Viterbo, Interference Cancellation and Iterative Detection for Orthogonal Time Frequency Space Modulation, IEEE Trans. Wirel. Commun. 17 (2018) 6501–6515.

[3] L. Jing, N. Zhang, C. He, J. Shang, X. Liu, H. Yin, OTFS underwater acoustic communications based on passive time reversal, Appl. Acoust. 185 (2022) 108386.

[4] Y. Xue, Y. R. Zheng, Orthogonal time-frequency space (OTFS) modulation for underwater mobile acoustic communications, J. Acoust. Soc. Amer. 154 (2023) A249–A249.

[5] L. Huang, Z. Zou, B. Wu, W. Wang, L. Ye, The effect of time-varying characteristics of shallow-sea waveguides on low-frequency acoustic signal transmission, Appl. Acoust. 229 (2025) 110375.

[6] S. Liu, H. Yan, L. Ma, Y. Liu, X. Han, UACC-GAN: A Stochastic Channel Simulator for Underwater Acoustic Communication, IEEE J. Ocean. Eng. 49 (2024) 1605–1621. doi:10.1109/JOE.2024.3401779.

[7] D. Sun, J. Wu, X. Hong, C. Liu, H. Cui, B. Si, Iterative double-differential direct-sequence spread spectrum reception in underwater acoustic channel with time-varying Doppler shifts, J. Acoust. Soc. Amer. 153 (2023) 1027–1041.

[8] K. Arunkumar, C. R. Murthy, Orthogonal Delay Scale Space Modulation: A New Technique for Wideband Time-Varying Channels, IEEE Trans. Signal Process. 70 (2022) 2625–2638.

[9] S. Hang, W. Li, OTFS for Underwater Acoustic Communications: Practical System Design and Channel Estimation, in: Proc. OCEANS, IEEE, 2022, pp. 1–7.

[10] L. Jing, C. Dong, C. He, W. Shi, H. Wang, Y. Zhou, Adaptive Modulation and Coding for Underwater Acoustic OTFS Communications Based on Meta-Learning, IEEE Commun. Lett. 28 (2024) 1845–1849. doi:10.1109/LCOMM.2024.3418192.

[11] X. Wang, X. Shi, J. Wang, Z. Sun, Iterative LMMSE-SIC Detector for DSE-Aware Underwater Acoustic OTFS Systems, IEEE Trans. Veh. Technol. 73 (2024) 9895–9910. doi:10.1109/TVT.2024.3362894.

[12] X. Guo, B. Wang, Y. Zhu, Z. Fang, S. Zhang, Underwater Acoustic Communication Based on OTFS-IM, in: Proc. 14th Int. Conf. Signal Process. Syst. (ICSPS), IEEE, 2022, pp. 216–219.

[13] X. Wang, X. Shi, J. Wang, J. Song, On the Doppler Squint Effect in OTFS Systems Over Doubly-Dispersive Channels: Modeling and Evaluation, IEEE Trans. Wirel. Commun. 22 (2023) 8781–8796.

[14] L. Jing, Z. Xue, C. He, W. Shi, H. Yin, A mobile underwater acoustic communication method based on orthogonal time frequency space modulation, Acta Acust. 49 (2024) 308–317.

[15] Q. Wang, N. Zhao, L. Jing, C. He, C. Zhou, A Low Complexity Turbo MMSE Equalization Method for OTFS Underwater Acoustic Communications, in: Proc. IEEE Int. Conf. Signal Process., Commun. Comput. (ICSPCC), IEEE, 2023, pp. 1–5.

[16] Z. Yuan, F. Liu, W. Yuan, Q. Guo, Z. Wang, J. Yuan, Iterative detection for orthogonal time frequency space modulation with unitary approximate message passing, IEEE Trans. Wirel. Commun. 21 (2021) 714–725.

[17] Z. Xue, Q. Wang, L. Jing, C. Zhou, C. He, Unitary approximate message passing detection method for otfs underwater acoustic communication system, in: Proc. IEEE Int. Conf. Signal Process., Commun. Comput. (ICSPCC), IEEE, 2023, pp. 1–5.

[18] Y. Zhang, S. Zhang, B. Wang, Y. Liu, W. Bai, X. Shen, Deep Learning-Based Signal Detection for Underwater Acoustic OTFS Communication, J. Mar. Sci. Eng. 10 (2022) 1920.

[19] S. Zhang, Y. Zhang, J. Chang, B. Wang, W. Bai, DNN-based Signal Detection for Underwater OTFS Systems, in: Proc. IEEE/CIC Int. Conf. Commun. China (ICCC Workshops, IEEE, 2022, pp. 348–352.

[20] T. Li, F. Zhou, L. Ma, X. Liu, M. Muzzammil, Multipath doa based mimo beamforming receiver scheme for high-rate underwater acoustic communications, Appl. Acoust. 221 (2024) 109994.

[21] H.-C. Song, An Overview of Underwater Time-Reversal Communication, IEEE J. Ocean. Eng. 41 (2015) 644–655.

[22] J. Yin, P. Du, J. Shen, L. Guo, Study on time reverse mirror in underwater acoustic communication, in: Proc. Mtgs. Acoust., volume 19, 2013, pp. 123–130.

[23] X. Pan, Z. Ding, J. Jiang, X. Gong, Robust time-reversal is combined with distributed multiple-input multiple-output sonar for detection of small targets in shallow water environments, Appl. Acoust. 133 (2018) 157–167.

[24] O. A. Godin, E. M. Uzhansky, T. Tan, B. G. Katsnelson, D. Y. Tan, T. Renucci, A. Voyer, R. M. McMullin, Acoustic characterization of the seabed with a single-element time-reversal mirror, Appl. Acoust. 210 (2023) 109442.

[25] C. Shi, L. Zhao, Y. Cui, Y. Chu, W. Guo, W. Wang, Joint Detection and Channel Estimation for MIMO-OTFS Systems, IEEE Trans. Veh. Technol. (2024).

[26] B. Li, S. Zhou, M. Stojanovic, L. Freitag, P. Willett, Non-uniform doppler compensation for zero-padded ofdm over fast-varying underwater acoustic channels, in: Proc. OCEANS, 2007, pp. 1–6. doi:10.1109/OCEANSE.2007.4302478.

[27] P. Raviteja, K. T. Phan, Y. Hong, Embedded pilot-aided channel estimation for otfs in delay–doppler channels, IEEE Trans. Veh. Technol. 68 (2019) 4906–4917.